Molecular Biology of the Cell
Vol. 17, 2942–2951, July 2006

A Distant Coilin Homologue Is Required for the Formation of Cajal Bodies in *Arabidopsis*[D]

Sarah Collier,*† Alison Pendle,*† Kurt Boudonck,*‡ Tjeerd van Rij,*§ Liam Dolan,* and Peter Shaw*

*John Innes Centre, Colney, Norwich NR4 7UH, United Kingdom; ‡CIIT Centers for Health Research, Research Triangle Park, NC 27709-2137; and §Institute of Biology, Leiden University, 2333 AL Leiden, The Netherlands

Submitted December 21, 2005; Revised April 11, 2006; Accepted April 12, 2006
Monitoring Editor: A. Gregory Matera

Cajal bodies (CBs) are subnuclear bodies that are widespread in eukaryotes, being found in mammals, many other vertebrates and in all plant species so far examined. They are mobile structures, moving, fusing, and budding within the nucleus. Here we describe a screen for *Arabidopsis* mutants with altered CBs and describe mutants that have smaller Cajal bodies (*ncb-2*, *ncb-3*), lack them altogether (*ncb-1*), have increased numbers of CBs (*pcb*) or have flattened CBs (*ccb*). We have identified the gene affected in the *ncb* mutants as a distant homolog of the vertebrate gene that encodes coilin (At1g13030) and have termed the resulting protein Atcoilin. A T-DNA insertional mutant in this gene (*ncb-4*) also lacks Cajal bodies. Overexpression of Atcoilin cDNA in *ncb-1* restores Cajal bodies, which recruit U2B″ as in the wild type, but which are, however, much larger than in the wild type. Thus we have shown that At1g13030 is required for Cajal body formation in *Arabidopsis*, and we hypothesize that the level of its expression is correlated with Cajal body size. The Atcoilin gene is unaffected in *pcb* and *ccb*, suggesting that other genes can also affect CBs.

INTRODUCTION

Cajal bodies (CBs) are subnuclear bodies first described in neuronal cells by Ramon y Cajal (1903) and designated nucleolar accessory bodies (see Gall, 2000, 2003; Ogg and Lamond, 2002; Matera, 2003; Shaw and Brown, 2004; Cioce and Lamond, 2005, for recent reviews). They were subsequently imaged by electron microscopy by Monneron and Bernhard (1969), who called them coiled bodies because they appeared to contain many coiled threads, but the name Cajal body has now been agreed in honor of their original discoverer. They have been identified in many but not all vertebrate cell types, and in all cell types so far examined in several species of monocot and dicot plants (Lafontaine, 1965; Beven *et al.*, 1995; Acevedo *et al.*, 2002). CBs have also been identified in *Xenopus* oocytes (Gall *et al.*, 1995). More recently an apparently similar nuclear body has been demonstrated in yeast cells (Verheggen *et al.*, 2001), and recent data show that analogous nuclear bodies are also present in *Drosophila* (J. G. Gall, personal communication). CBs have been shown to be dynamic structures, moving, fusing together, and splitting apart within the nucleus and occasionally within the nucleolus (Boudonck *et al.*, 1999; Platani *et al.*, 2000).

This article was published online ahead of print in *MBC in Press* (http://www.molbiolcell.org/cgi/doi/10.1091/mbc.E05–12–1157) on April 19, 2006.

[D] The online version of this article contains supplemental material at *MBC Online* (http://www.molbiolcell.org).

† These authors contributed equally to this work.

Address correspondence to: Peter J. Shaw (peter.shaw@bbsrc.ac.uk).

Abbreviation used: CB, Cajal body.

CBs contain a very wide variety of different proteins and small RNAs, both small nuclear (snRNAs) and small nucleolar (snoRNAs), along with their associated protein complexes, as well as telomerase (Zhu *et al.*, 2004; Cioce and Lamond, 2005). They also contain scaRNAs–small RNAs that are specifically targeted to CBs—and are involved in directing modifications of snRNAs and snoRNAs (Jady and Kiss, 2001; Darzacq *et al.*, 2002). Many of the proteins, such as fibrillarin and dyskerin/cbf5p, are shared with the nucleolus, in line with Ramon y Cajal's original description of CBs as nucleolar accessory bodies. The various constituent proteins and RNA species dynamically move in and out of the CBs, showing that these factors transit through rather than being stably stored in this compartment (Sleeman *et al.*, 2003; Dundr *et al.*, 2004). To date, the biochemical data, although still far from complete, suggest that CBs have a range of functions centered around the maturation of RNA species and the assembly of transcription-related complexes. For example, CBs have been shown to have a role in the recycling/assembly of the U4/U6/U5 tri-snRNP, because RNAi knockdown of specific factors necessary for tri-snRNP assembly causes U4/U6 di-snRNP to accumulate in CBs (Schaffert *et al.*, 2004). Fluorescence resonant energy transfer (FRET) microscopy has further shown the assembly of the U4/U6 di-snRNP occurring in CBs (Stanek and Neugebauer, 2004). A role for CBs in the maturation of U2 snRNP has also been shown (Nesic *et al.*, 2004).

Vertebrate CBs are highly enriched in coilin, a protein of unknown function that is considered diagnostic of this type of nuclear body (Andrade *et al.*, 1991; Raska *et al.*, 1991). *Xenopus* has a closely related homologue to coilin, which again is localized in *Xenopus* CBs (Tuma *et al.*, 1993). A mouse insertional mutant in the coilin gene had markedly altered CBs, termed residual CBs, which failed to recruit CB constituent proteins such as SMN (Tucker *et al.*, 2001). The

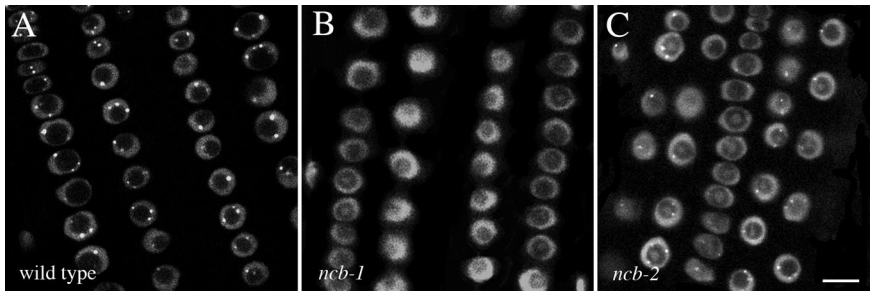

Figure 1. Confocal images of wild-type (1214), *ncb-1* and *ncb-2* root epidermal tissue. All lines express U2B″:GFP. (A) In the parental line all nuclei show clear, bright nuclear foci corresponding to CBs, as well as a lower level of nucleoplasmic labeling. The label is mostly excluded from the nucleolus. (B) In *ncb-1* no CBs are visible and the nucleoplasmic labeling is generally brighter than in the parental line. Labeling is often visible in the central regions of the nucleoli. (C) In *ncb-2*, many nuclei show CB foci, but these are significantly smaller than in the parental line. The nucleoplasm and the central region of the nucleoli are labeled. Bar, 10 μm.

mutant mice had a reduced litter size, but were otherwise apparently normal. A distant potential homologue to coilin in the *Arabidopsis* genome has been noted (Tucker and Matera, 2005), but the degree of similarity is very low (E = 0.05), and neither the gene nor its product have been previously characterized.

Here we describe results from a fluorescence microscopy–based mutant screen of an *Arabidopsis* line engineered to express GFP in CBs and show the CB phenotypes of the six mutants identified. We further demonstrate that three *no cajal bodies* (*ncb*) mutants have mutations in At1g13030, which we identify as a distant homologue of the vertebrate coilin gene. *ncb-1* lacks any detectable CBs, whereas *ncb-2* and *ncb-3* have smaller CBs than wild type. Stable expression of a fusion of At1g13030 with red fluorescent protein in the *ncb-1* background restores nuclear bodies in all cell types, verifying that mutations in the At1g13030 gene are responsible for the *ncb-1* phenotype. Furthermore these CBs recruit the spliceosomal U2B″-GFP, suggesting that the restored bodies are functional. Interestingly the CBs induced in this way are much larger than native CBs.

MATERIALS AND METHODS

Plant Materials and Growth Conditions

Arabidopsis thaliana seeds were sterilized in 5% bleach for 10 min and washed with water three times. These seeds were sown in Petri-dishes containing 1× Murashige and Skoog (MS) plant salt mixture supplemented with 0.5% phytagel and 1% glucose. Before germination, seeds were stratified at 4°C for 48 h and then grown in a standard growth cabinet (25°C, constant light). When mature they were moved onto compost and grown in the greenhouse under long day conditions (16 h photoperiod).

EMS Mutagenesis

Previously the full-length (693 base pairs) potato U2B′ cDNA fused in frame to the 5′ end of sGFPS65T under the control of the 35S promoter was transformed into *Arabidopsis*, Colombia ecotype, to generate the line used in this study (line 1214; Boudonck *et al.*, 1999). Seeds homozygous for the U2B′:GFP construct were subjected to ethyl methanesulfonate (EMS) mutagenesis. The seeds were incubated in 30 ml 0.1% Tween-20 for 48 h at 4°C, followed by 8-h incubation in 20 ml 0.5% (wt/vol) EMS. The seeds were washed three times in water and then transferred into 2 l of water and stirred overnight. The mutagenized seed (M1) was sown on soil and grown in the glasshouse, and the M2 seed was harvested. Four separate batches of mutagenized U2B′:GFP seed were collected.

Screening for Cajal Bodies

The EMS M_2 population of seed generated from the U2B′:GFP *Arabidopsis* line (1214) was used in the screen. To obtain the longer roots and hypocotyls needed for screening, seeds were sown in a row across Petri-dishes containing MS phytagel solid media. After a 48-h stratification at 4°C, they were germinated in a standard growth cabinet (25°C, constant light) with the plates inclined at a 90° angle, allowing roots to grow along the surface of the medium. After 36 h, they were covered with a black plastic bag, which was removed 48 h later. Seedlings were grown for a further 5 d in the light before being screened. Eight-day-old seedlings in a row across a Petri dish were covered with 0.5 ml MS liquid media (3% [wt/vol] sucrose and 4.4 g/l Murashige and Skoog medium with vitamins, pH 5.8; Imperial Laboratories, Andover, United Kingdom) and a coverslip. The hypocotyl cells of the seedlings were then examined for abnormalities in the GFP-labeled CBs using a Nikon Eclipse E600 epifluorescence microscope with a 100×/1.4 Nikon Plan Apo objective (Nikon UK, Kingston upon Thames, United Kingdom). It was important not to cover leaves with immersion oil, which kills the seedlings, and it was important to use minimal exposure to the microscope illumination. Those with abnormal CBs were moved to fresh plates and returned to the growth room until large enough to be transplanted on to soil in the greenhouse. Putative mutants were grown to maturity, and the M3 seedlings rescreened to ensure the line was stable and homozygous.

Mapping

A segregating F2 population was made by crossing a plant homozygous for the *ncb-1* mutation in ecotype Columbia background (Col) and a wild-type ecotype Landsberg erecta (Ler) plant. Mapping was then carried out according to the procedure described by Bell and Ecker (1994).

Primers Used

Primers used were as follows: At1g13030: F1: GTGAGGGTTCGTCTGGTGTT; R3: AGCCTTCTTCTCTGGCACAA: F9: ATGGGGCACAGAGAAGTCAGG; R10: TCAATGAGGCGGTATGC; R12: TGGTCAGGCTCGGGCAGTG and F-At1g13030: TGCTTTTGTGGATTGCAGGTC; R-At1g13030: GAAACTGTGAGGAGCCTTGC.

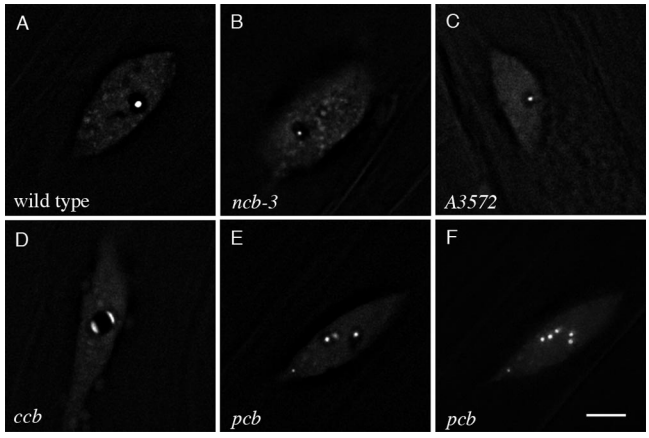

Figure 2. Visualization of U2B″:GFP labeling in four other mutants identified. In each case a typical hypotocotyl cell is shown, imaged by wide-field CCD microscopy followed by image deconvolution. (A–E) Single *z* sections; (F) a *z* projection. (A) Wild type (1214) shows a single, clear CB. *ncb-3* (B) and A3572 (C) both have significantly smaller CBs, similar to *ncb-2*. (D) *ccb* displays flattened CCBs around the nucleolar periphery. (E) *pcb* has an increased number of CBs. (F) Projection of the entire nucleus shown in E to clearly show the increased number of CBs. (There are no additional CBs besides those shown for the other lines.) Note that, in contrast to the rapidly dividing root cell nuclei, shown in Figure 1, the nuclei of many elongated plant cells are themselves elongated. Bar, 5 μm.

Sequencing Primers

Sequencing primers used were as follows: Coilin-1f: CTGTGCGTTTACAG-CATCAAA; Coilin-1r: GAAGATGGATCCCTGGAGGT; Coilin-2f: TTAC-CTTTTGCAGGGGTTTG; Coilin-2r: TTACTACCCCCAGCAGGTTG; Coilin-3f: TGAGGCGGTATGCAATAACA; Coilin-3r: AGATCACCAAGCAACCAAGG; Coilin-4f: GAAACTGTGAGGAGCCTTGC; Coilin-4r: TGCTTTTGTGATTG-CAGGTC; Coilin-5f: TGGCACAGATCGTTATGCTC; Coilin-5r: TGGAGATT-GTTGGGGAAGAC; Coilin-6f: AGCCTTCTTCTCTGGCACAA; Coilin-6r: GT-GAGGGTTCGTCTGGTGTT; Coilin-7f: AGAGAGAGGCCATGAGGACA; and Coilin-7r: AGAAGACGAAGGCTCCAACA.

cDNA Preparation and Expression Analysis

RNA from flower buds of the parental 1214 line and *ncb-1* and *ncb-2* plants was prepared using the TRI method. Briefly, tissue was ground in liquid nitrogen and then TRI reagent (Sigma, Poole, Dorset, United Kingdom) was added; then the mixture was vortexed and allowed to extract for 10 min. The sample was then extracted with chloroform, the aqueous phase was collected, and RNA was precipitated with isopropanol, washed in 70% ethanol, and resuspended in DEPC (diethyl pyrocarbonate)-containing water. Reverse transcription was carried out using Abgene Reverse-IT First Strand Synthesis Kit (Abgene, Epsom, United Kingdom) to generate cDNAs of each sample. Then standard Taq PCR was performed using coilin primers F9 and R10 and F9 and R12 spanning the mutation sites. The PCR products were excised from the gel and then cloned using the Topo II cloning system (Invitrogen, Paisley, United Kingdom). DNA from single colonies was sequenced using standard procedures. Primers for purification of full-length At1g13030 and ligation into Gateway entry vector were designed and used as described by Koroleva *et al.* (2005). The mRFP Gateway destination vector was a gift from John Brown and Sang Hyon Kim (Scottish Crop Research Institute, Dundee, Scotland).

T-DNA Insertion Line Analysis

Line 233HO2 was obtained from the GABI/kat collection (http://www.gabi-kat.de/). DNA was prepared from approximately 50 individual plants of the line and screened for homozygous insertion by PCR using T-DNA left border and forward and reverse primers specific for gene At1g13030 (F-At13030 and R-At13030). A plant homozygous for the insertion was selected, and seed from this plant was collected. cDNA was prepared from the homozygous line in the same manner as described above for the parental and mutant lines and was analyzed by PCR using a primer pair (F1 and R3) before the T-DNA insertion and a primer pair (F9 and R12) after the insertion.

Microscopy and Image Processing

Immunofluorescence labeling was carried out using 4G3 antibody against U2B″ or 72B9 antibody against fibrillarin as described by Boudonck *et al.* (1999). Samples were imaged with a Nikon Eclipse 600 epifluorescence microscope equipped with a Hamamatsu ORCA-ER cooled CCD camera (Bridgewater, NJ) and a Prior Proscan *x,y,z* stage using Metamorph software (Universal Imaging, West Chester, PA) and were processed using ImageJ, a public domain image processing program written by Wayne Rasband and obtainable from http://rsb.info.nih.gov/ij/ and Photoshop7 (Adobe, San Jose, CA). Image deconvolution of 3D *z* series was carried out using Autodeblur (Autoquant Imaging, Troy, NY). Confocal microscopy was carried out using a Leica SP confocal microscope (Leica Microsystems UK, Milton Keynes, United Kingdom).

Section Preparation and Transmission Electron Microscopy

Three-day-old seedlings were fixed overnight in a 2.5% glutaraldehyde in 0.05 M cacodylate buffer, pH 7.2. Samples were washed three times in 0.05 M sodium cacodylate for 15 min and postfixed in 1% osmium tetroxide for 1 h followed by three 15-min washes in 0.05 M sodium cacodylate. Samples were dehydrated for 1 h in each of the serial ethanol dilutions: 30, 50, 70, 90, and 100%. Samples were then infiltrated for 1 h with LR white resin (Agar Scientific, Stansted, United Kingdom) resin:ethanol 1:1, 2:1, 3:1, 100% resin, and finally 100% resin overnight. Samples were then polymerized in fresh resin at 60°C for 16 h. sections of 100 nm were made on an ultramicrotome (Reichert Ultracut E, Leica Microsystems UK) using a 45° glass knife. Samples were picked up with carbon-coated 200-mesh hexagon copper/palladium grids (Agar Scientific), air dried, and stained with 2% aqueous uranyl acetate for 1 h and 1% lead citrate for 30 s. TEM images were obtained using a JEOL 1200 transmission electron microscope (JEOL UK, Welwyn Garden City, United Kingdom). TEM images were recorded using a Deben AMT 1.3K digital camera system and subsequently processed for publication using Adobe Photoshop7 (Adobe, San Jose, CA).

RESULTS

Screening and Identification of CB Mutants

In the U2B″:GFP line (1214), the fusion protein is present within the CBs at a high concentration and also localizes at a lower concentration to the rest of the nucleoplasm, but not the nucleolus. Overexpression of the U2B″:GFP fusion protein was shown to have no detectable effect on the growth or development of the plants (Boudonck *et al.*, 1999).Therefore, it was deemed a good marker line in which to generate, identify, and study living plants with mutated CBs. CBs in *Arabidopsis* are spherical and often found in close association with the nucleolus. In the hypocotyl cells, the cell type used in the screen, the nuclei are large and usually contain a single CB ~1 μm in diameter. Two batches of seed were treated with EMS and then grown to maturity. The resulting M_2 seed was then screened for abnormal CBs by epifluorescence microscopy of the seedling hypocotyl cells. M_2 families were examined from the first series and the second series (n = 725 and 510, respectively), a total of 1235 separate lines. From these, six separate CB mutants were identified, a fre-

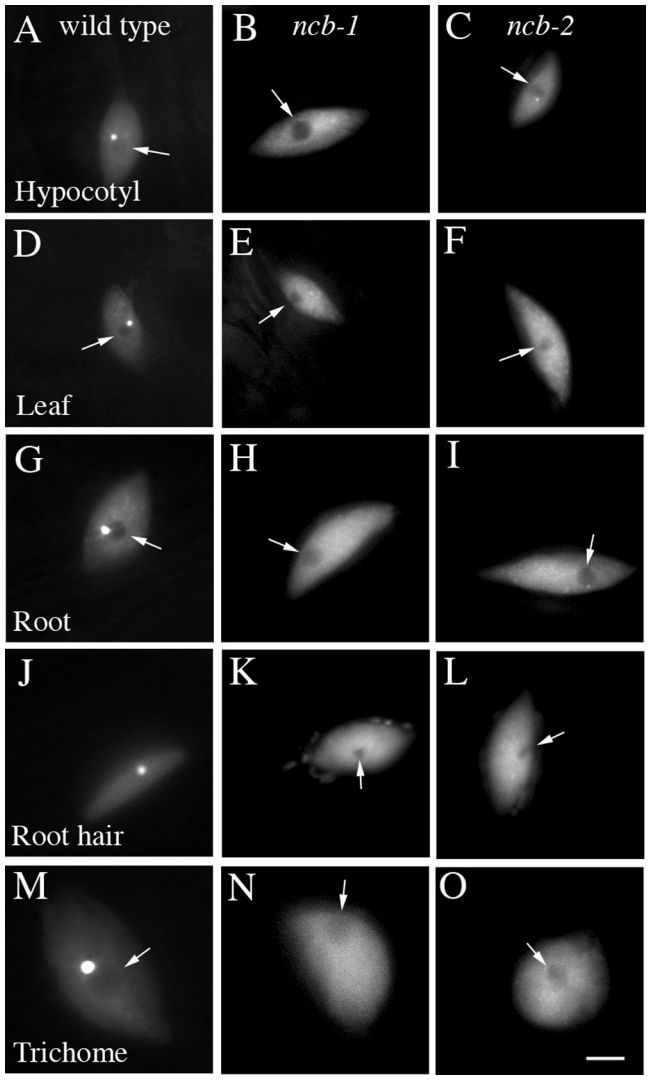

Figure 3. Visualization of U2B″:GFP labeling in different cell types of wild type (1214; left-hand column), *ncb-1*(middle column), and *ncb-2* (right-hand column). (A–C) Hypocotyl cells. (D–F) Leaf epidermal cells. (G–I) Root epidermal cells. (J–L) Root hair cells. (M–O) Trichome cells. In all cell types examined, whereas the parental line shows bright, clear CBs, in *ncb-1* CBs are not visible, and in *ncb-2* CBs are either much reduced in size or absent. All images were collected by wide-field epifluorescence using a CCD camera. The arrows indicate the nucleoli. Bar, 5 μm.

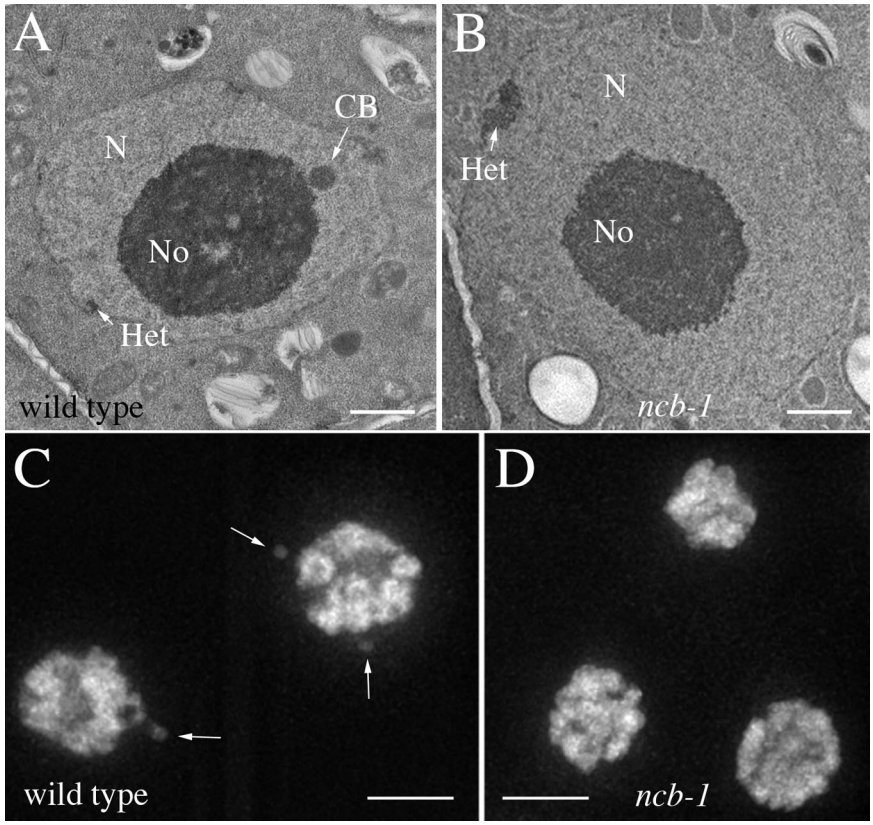

Figure 4. Transmission electron microscopy and anti-fibrillarin labeling of root nuclei. (A) EM of parental (1214) line showing a clear CB (arrow) next to the nucleolus. (B) *ncb-1* never shows visible CBs in the EM. N, nucleus; No, nucleolus; Het, heterochromatin. Bar, 1 μm in A and B. (C) Parental (1214) line also shows clear CBs in every nucleus after immunofluorescence labeling with anti-fibrillarin (arrows). (D) In *ncb-1* no CBs are visible. (*z* projections of deconvoluted wide-field image stacks). Bar, 5 μm in C and D.

quency of 0.5%. These included mutants with smaller or no visible CBs, multiple CBs, and cap-shaped CBs. In this article we characterize two distinctive CB phenotypes. The first mutant has no visible CBs in any cell type examined (Figure 1B); the second has a very similar phenotype, but often shows small CBs (Figure 1C). These mutants were later shown to be allelic to each other and were named *no cajal body 1* (*ncb-1*), and *no cajal body 2* (*ncb-2*). Both the mutants segregate in 3:1 ratio, indicating that they are caused by recessive loss-of-function mutations at a single allele. These two mutant lines were back-crossed to the parental 1214 line three times before further analysis and mapping of the mutations. Neither of these lines showed any significant growth defects when compared with the parental line.

The four other mutants obtained are shown in Figure 2 compared with the parental 1214 line (Figure 2A). The mutant line shown in Figure 2B had smaller CBs and was later also shown to be an *ncb* allele and was named *ncb-3*. The mutant in Figure 2C (A3572) also has smaller CBs, but has not so far been fully analyzed genetically. The line in Figure 2D frequently shows flattened or cap-shaped CBs and was named *ccb* (*cap-shaped Cajal bodies*). The mutant in Figure 2E has an increased number of CBs. This is made clearer by the 3D projection of the entire nucleus shown in Figure 2F. This mutant was named *pcb* (*poly Cajal bodies*). The hypocotyl cells used in this screen usually showed one, or sometimes two, CBs in the parental line (mean = 1.06, SD = 0.25, n = 16). The *pcb* mutant showed significantly more CBs (mean = 5.9, SD = 1.55, n = 8). The numbers of CBs did not differ significantly from the parental line in any mutants apart from *pcb* and *ncb-1*. (*ncb-2*: mean = 1.25, SD = 0.62, n = 12; *ncb-3*: mean = 1.14, SD = 0.34, n = 7; *ccb*: mean = 1.6, SD = 0.55, n = 5; A3572: mean = 1.7, SD = 0.76, n = 7).

Phenotypic Analysis of ncb-1 and ncb-2

Nuclei from different cell types (hypocotyl, leaf, root, root hair, trichome) of *ncb-1* and *ncb-2* mutants are shown in Figure 3 compared with the wild-type parental line. In *ncb-1*, CBs are never seen, whereas in *ncb-2*, small CBs are often visible. In both mutants, the nucleoplasmic GFP fluorescence appears greater than in the parental wild type. It is possible that this CB phenotype is due either to the absence or reduction of CBs themselves or to a failure of CBs to recruit the GFP-U2B″ as in the wild type. We therefore examined ultrathin sections of wild-type (1214) and *ncb-1* root tissue by transmission electron microscopy. Because CBs are preferentially associated with nucleoli, we examined nuclei sectioned in a plane such that the nucleolus was clearly visible. On the basis of only this criterion, we randomly selected and photographed 38 wild-type nuclei and 39 *ncb-1* nuclei and scored each image for the presence of one or more CBs. Because CBs are small compared with the size of the nucleus, not all wild-type nuclei contained a CB within the plane of the section, although fluorescence microscopy shows that all root nuclei contain CBs (Boudonck *et al.*, 1999). In fact, of the 38 wild-type cells, 10 (26%) contained a clearly identifiable CB (e.g., Figure 4A). Of the 39 *ncb-1* cells, none contained a clearly identifiable CB (e.g., Figure 4B). If we take 26% as the probability of visualizing a CB in a background that contains CBs, that is a probability of 74% of missing CBs when they are present. This means that the probability of missing CBs in 39 *ncb-1* sections assuming the null hypothesis (that they are present) is 0.74^{39} or 7.9×10^{-6}—a very small probability. We therefore conclude that *ncb-1* lacks ultrastructurally identifiable CBs by the criterion of electron microscopy as well as by GFP-U2B″ labeling.

A) Amino acid sequence of AtCoilin

```
MEEEKVRVRLVFEDRRILSKYQKKQGLTRSWVVLNRKCHRTISEFSDHIFHTFSLCEACPHGLSLSMEGFVLPPFESSCV
1        10        20        30        40        50        60        70        80
LKDKDIVCVKKKKESLLEIVGEDSDENVYNAIEVEERPQIRPGEMLLANEEFQKETGGYESESEEDELEEEAEEFVPEKK
        90       100       110       120       130       140       150       160
ASKKRKTSSKNQSTKRKKCKLDTTEESPDERENTAVVSNVVKKKKKKKSLDVQSANNDEQNNDSTKPMTKSKRSSQQEES
       170       180       190       200       210       220       230       240
KEHNDLCQLSAETKKTPSRSARRKKAKRQWLREKTKLEKEELLQTQLVVAPSQKPVITIDHQATKEKHCETLENQQAEEV
       250       260       270       280       290       300       310       320
SDGFGDEVVPVEVRPGHIRFKPLAGTDEASLDSEPLVENVLWNGNMTKKKGQKWGTEKSGFSKRYAQDFNEDATTQPAEA
       330       340       350       360       370       380       390       400
ETLANCPIDYEQLVAYTGSVKKGDVIAYRLIELTSSWTPEVSSFRVGKISYYDPDSKMVTLMPVQEFPIEKKTEEDDDFC
       410       420       430       440       450       460       470       480
MQPDTSLYKEDGSLEIEFSALLDVRSVKTSSSDSAEVAKSALPEPDQSAKKPKLSANKELQTPAKENGEVSPWEELSEAL
       490       500       510       520
SAKKAALSQANNGWNKKGSSSGGSWSYKALRGSAMGPVMNYLRSQKEI
```

B) Alignment of AtCoilin amino acid residues 1-100

```
                    . .*::* *:                  *:::: :  *.:::: . * . :
Xenopus_laevis      --MAAPSPVRVKLLFDYP-----PPAIPESCMFWLLLDAKRCRVVTDLASIIRHKYMNGQ
Danio_rerio         MATSSFNTARVRLYFDYP-----PPATPECRMCWLLVDLNKCRVVADLSSIIKEKFGYSR
Homo_sapiens        --MAASETVRLRLQFDYP-----PPATPHCTAFWLLVDLNRCRVVTDLISLIRQRFGFSS
Mus_musculus        --MAASETVRLRLQFDYP-----PPATPHCTVFWLLVDLNRCRVVTDLISLIRQRFGFSS
Arabidopsis         ---MEEEKVRVRLVFEDRRILSKYQKKQGLTRSWVVLNRKCHRTISEFSDHIFHTFSLCE
                       1        10        20        30        40        50

                         :.* :*   **. **  :::*:* : ** .      .
Xenopus_laevis      GG--GISLYVEDCLLPPGESILVIRDNDSIRVKWDGAAIERNQEAETCNDGAQNKSKKRH
Danio_rerio         KT--ILDLFIEECYLPSAESIYIVRDNDSVRVKVSCPVQVNGTEAEAQNS----KSKKRG
Homo_sapiens        GA--FLGLYLEGGLLPPAESARLVRDNDCLRVKLEERGVAENSVVISNGDINLSLRKAKK
Mus_musculus        GA--LLGLYLEGGLLPPAESARLVRDNDSLRVKLEDQGLPENLIVSNGGDSSFPCRKAKK
Arabidopsis         ACPHGLSLSMEGFVLPPFESSCVLKDKDIVCVKKKESLLEIV-----------------
                     60        70        80        90       100
```

C) Alignment of AtCoilin amino acid residues 409-511

```
                       **  *   :..   *. **::*:*::..::*:**.:: *:*  .:* ::   :  :.
Xenopus_laevis      QETMKRDYSSLPLLAAAPQVGKLIAFKLLEVSENYTPEVSEYKEGKILSFDPVTKQIEMEIIS
Danio_rerio         ELAPKRDYATLPLLAAPPAVGQKIAFKLLELTENYTPEVSDYKEGKILAFNPQTKVTELELLS
Homo_sapiens        VETPKKDYSLLPLLAAAPQVGEKIAFKLLELTSSYSPDVSDYKEGRILSHNPETQQVDIEILS
Mus_musculus        VEPPKKDYSLLPLLAAAPQVGEKIAFKLLELTSDYSPDVSDYKEGKILSHDPETQQVDIEVLS
Arabidopsis         ------DYEQLVAYTGSVKKGDVIAYRLIELTSSWTPEVSSFRVGKISYYDPDSKMVTLMPVQ
                          410       420       430       440       450       460

                         :. : * .  . :     * .      :   :  *:: * :
Xenopus_laevis      -QQTMRKPGKFDVVYQSEDEEDIVEYAVPQESKVMLNWNTLIEPRLLMEKESQVQC----
Danio_rerio         RPQAPAEPGKFDLVYQNPDGSERVEYAVTQGSQLTERWDSLLEPRLIVENAE--------
Homo_sapiens        SLPALREPGKFDLVYHNENGAEVVEYAVTQESKITVFWKELIDPRLIIESPSNTSSTEPA
Mus_musculus        SLPALKEPGKFDLVYHNENGTEVVEYAVTQEKRITVLWRELIDPRLIIDSSGSISST---
Arabidopsis         EFPIEKKTEEDDDFCMQPDTSLYKEDGS-----LEIEFSALLDVRSVKTSS---------
                      470       480       490            500       510
```

Figure 5. Comparison of Atcoilin with vertebrate coilins. (A) The entire sequence of Atcoilin, with regions of significant homology with vertebrate coilin highlighted in green. (B) Alignment of Atcoilin residues 1–100 and vertebrate coilins. (C) Alignment of Atcoilin residues 409–511 and vertebrate coilins.

The absence of CBs in *ncb-1* was further confirmed by labeling of fibrillarin, which is located in both CBs and the dense fibrillar component of the nucleolus. Examples are shown in Figure 4, C and D. All labeled nuclei from the wild type showed clear CBs (arrows in Figure 4C), whereas no CBs could be identified in the *ncb-1* mutant (Figure 4D).

Identification of the NCB Gene

The *NCB* gene was isolated using a map-based cloning strategy. A segregating F2 population was made by crossing a plant homozygous for the *ncb-1* mutation (in ecotype Columbia background; Col) and a wild-type ecotype Ler (Landsberg erecta) plant. Plants from this population were phenotyped by fluorescence microscopy and genotyped by PCR using characterized markers (Bell and Ecker, 1994). The mutation was initially mapped to the top of chromosome 1 between the SSLP (single sequence length polymorphism) markers nga59 and nga392 (Bell and Ecker, 1994), using a population of 100 chromosomes. The markers nga126 and AthCHIB on chromosome 3 also gave a low recombination frequency, indicating that this region may contain the U2B″:GFP transgene. Analysis of a further 560 chromosomes identified a single recombination event between the SSLP markers F3F19–935 and F3F19–941 on chromosome 1, but no recombination between F3F19–935 and *ncb-1*. On the other side of the mutation, 10 recombination events occurred between T28P6 and *ncb-1*. The gene At1g13030, which has some similarity to the human coilin gene (Figure 5; Tucker and Matera, 2005), is located in the interval between T28P6 and F3F19–935. We therefore sequenced the genomic region containing At1g13030 from the *ncb-1* background. When compared with the wild-type sequence, a single base change from G to A was found at the 3′ splice site at the beginning of exon 12 (Figure 6).

Initial mapping of *ncb-2* also positioned it at the top of chromosome 1, with no recombination at the SSLP marker F3F19–935. F1 seedlings from a cross between *ncb-1* and *ncb-2* showed the *ncb-2* phenotype, indicating that the two mutations are allelic. We therefore sequenced At1g13030 from *ncb-2* and again found a single base change from G to A, at the 5′ end of exon 9 (Figure 6A).

Finally, we sequenced At1g3030 in the other four mutants identified in the screen. One of them, which we then named *ncb-3*, is another allele and contains a single base change from G to A at position 320. This is predicted to change glutamate E106 to lysine. In line A3572 (Figure 2C), only primer pairs coilin-2r/f and coilin-3r/f produced a PCR product; the other primer pairs used for sequencing the gene

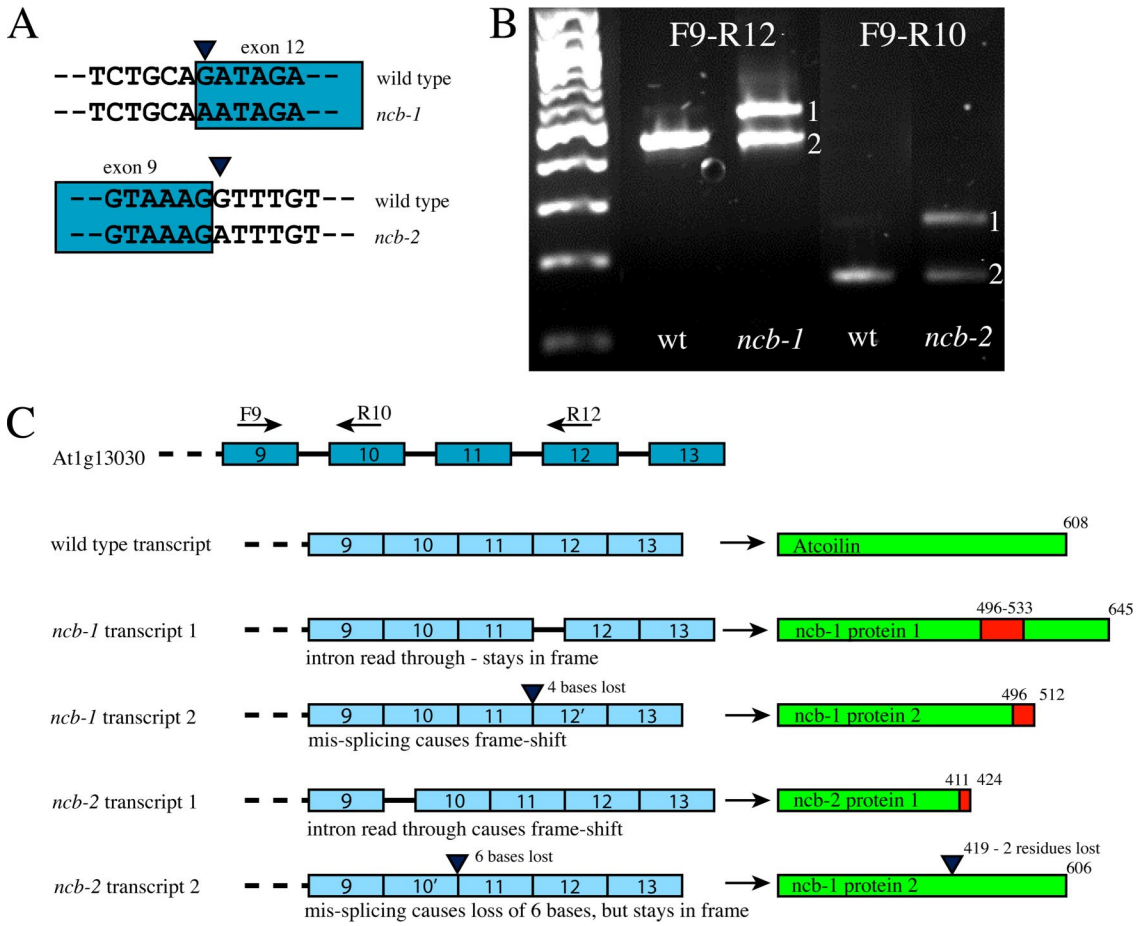

Figure 6. Diagram showing the location of the base changes and transcript analysis of *ncb-1* and *ncb-2*. (A) In *ncb-1* a change from G to A has occurred at the 5′ end of exon 12. In *ncb-2* a change from G to A has occurred at the 3′ end of exon 9. (B) RT-PCR of wild type (1214), *ncb-1* and *ncb-2* mRNA. Lane 1, markers. Lane 2, wild type with primers F9 and R12 shows a single band of the predicted size. Lane 3, *ncb-1* with primers F9 and R12 shows two bands, one of about the same size as the wild type and one significantly larger. Lane 4, wild type with primers F9 and R10 shows a single band of the predicted size. Lane 5, *ncb-2* with primers F9 and R10 shows two band, one of about the same size as the wild type and one significantly larger. (C) Diagram of the transcripts of wild-type cDNA from At1g13030 and the two transcripts from each of *ncb-1* and *ncb-2* and of the predicted polypeptides from each transcript. In the predicted proteins, the wild-type residues are shown in green, with the aberrant residues in red.

in all the other mutants and in the wild type failed to amplify PCR products. This suggests a complex rearrangement or deletion in the gene. Sequence analysis showed that At1g13030 was unaffected in *ccb* and *pcb*. It is therefore probable that these mutant phenotypes are caused by other loci.

Analysis of T-DNA Insertional Mutant

Because At1g13030 was identified as the gene responsible for *ncb-1*, *ncb-2*, and *ncb-3*, we searched publicly available collections for T-DNA insertions into this gene. Line 233H02 from the GABI-Kat collection was annotated as having a T-DNA insertion into exon 7 of At1g13030. We obtained this line and verified the insertion site by PCR analysis, using primers from each side of the insertion site (to determine the direction of the insertion) and from the left border of the T-DNA sequence. Plants from this line were then screened by PCR to identify plants homozygous for the insertion, and seed was collected from a homozygous plant for further analysis.

We carried out immunofluorescence analysis of CBs in seedlings homozygous for the insertion using 4G3 antibody, which is specific for U2B″ and which we have previously shown localizes CBs clearly in plants (Beven *et al.*, 1995). No CBs are visible in plants homozygous for the T-DNA insertion, as shown by immunofluorescence labeling in Figure 7. We designated this mutation *ncb-4*. Therefore we have identified four independent mutations in At1g13030, and each confers a defective CB phenotype. This confirms that At1g13030 is required for CB formation.

Expression Analysis

The single base changes in both *ncb-1 and ncb-2* occurred at splice sites in At1g13030: the 3′ end of exon 12 for *ncb-1* and the 5′ end of exon 9 for *ncb-2*. We therefore predicted that the mRNA in the two mutants would be incorrectly spliced. To test this, we purified polyA mRNA and made cDNA from the parental (1214) line and from each mutant. These were then analyzed by PCR, using a forward primer in exon 9 (F9) and reverse primers in exons 10 and 12 (R10 and R12). The results of this analysis are shown in Figure 6B. As expected, the wild type showed a single band for each primer pair of the expected size for the spliced mRNA. However, each mutant showed two bands of about the same intensity, in

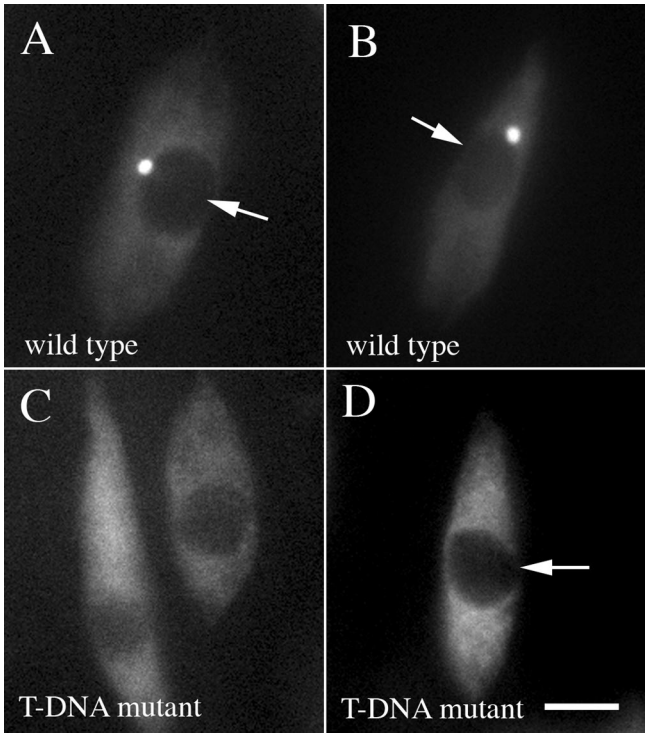

Figure 7. Immunofluorescence labeling of CBs in parental (1214) line and T-DNA insertional mutant GABI-Kat line 233H02 in At1g13030. Root tissue was labeled with antibody 4G3, specific for U2B″. Images collected by wide-field epifluorescence using a CCD camera. (A and B) In the parental line CBs are clearly seen. (C and D) In the insertion line no CBs are seen. Arrows indicate the nucleoli. Bar, 5 μm.

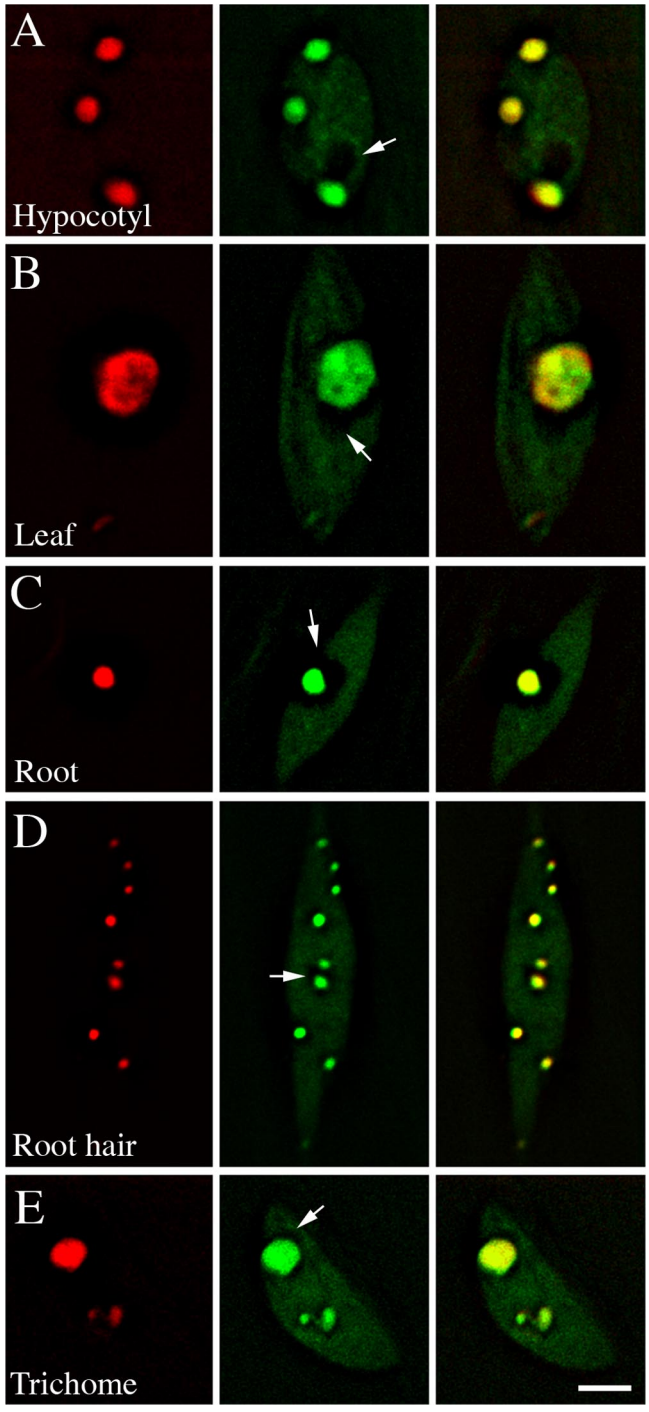

Figure 8. CBs in an *ncb-1* line in which mRFP:Atcoilin is over expressed using the 35S promoter. Single optical sections from 3D CCD data after deconvolution. The different cell types correspond to those shown for the parental (1214) line, *ncb-1* and *ncb*-2 in Figure 3. Left-hand panels show coilin:mRFP; center panels, U2B″:GFP; right-hand panels, overlay. In all cells the CBs are greatly enlarged and in some cells are also more numerous than in the wild type. (A) Hypocotyl cell. (B) Leaf epidermal cell. (C) Root epidermal cell. (D) Root hair cell. (E) Trichome cell. Arrows show the presumed location of nucleoli. Bar, 5 μm.

each case one of about the wild-type size, and one significantly larger. We cloned and sequenced each band for each mutant. Figure 6C shows in diagrammatic form the transcripts identified (the actual sequences are shown in Supplementary Figure 1). In the case of *ncb-1*, for the smaller band, the intron between exons 11 and 12 has been excised, but the splicing has been mis-targeted, resulting in four additional bases being lost from the 5′ end of exon 12 in the spliced mRNA. In the larger band, this intron has not been removed and remains in the mRNA. In the case of *ncb-2*, the intron between exons 9 and 10 has been mis-spliced in the smaller band, resulting in the loss of six bases from the 3′ end of exon 9, whereas in the larger band, this intron remains in the mRNA.

The predicted consequences of these mis-spliced mRNAs when translated into protein are shown in diagrammatic form in Figure 6C and in detail in Supplementary Figure 2. The wild-type protein has 608 amino acid residues. For *ncb-1*, the 4 bases lost in the shorter mRNA will introduce a frame shift after residue 493, and a stop codon in this frame will terminate translation after 39 extraneous residues. In the case of the longer, intron-containing mRNA, 37 extra residues will be translated from the intron starting at residue 496. There is no stop codon in the intron in this reading frame, and translation will continue back into the correct frame at the start of exon 12, giving a polypeptide of 645 residues with the correct start and finish, but with extraneous residues internally inserted after residue 493. For *ncb-2* the shorter mRNA, missing 6 bases would simply cause 2 residues to be deleted (420 and 421, valine and lysine, respectively, in the wild-type protein). The longer mRNA containing the intron would translate 5 amino acid residues

from the intron before encountering a stop codon, generating a truncated protein of 424 residues.

mRNA from the T-DNA insertional mutant *ncb-4* was also analyzed in the same way (unpublished data). The insertion was in exon 7 of At1g13030, and the cDNA from the homozygous *ncb-4* plants was analyzed by PCR using primer pairs before (F1 and R3) and after (F9 and R12) the insertion site. Both primer pairs gave clear, single PCR products, showing that transcription progressed through the T-DNA insertion. Translation would be predicted to progress through to exon 7 of the gene and to terminate at a stop codon in the T-DNA sequence. Thus, the N terminal sequence from At1g13030 would be predicted to be expressed, but to end prematurely within exon 7 with extraneous residues at the C-terminus.

Overexpression of NCB/At1g13030 Results in the Formation of Larger CBs

Given that plants homozygous for loss-of-function *ncb* alleles have either smaller or no CBs, we predicted that plants overexpressing NCB/At1g13030 should have larger CBs. Full-length cDNA for At1g13030 was prepared by PCR from a cDNA library, cloned into a Gateway entry vector, and then transferred to a plant binary destination vector designed to express mRFP N-terminal fusions under the 35S promoter (Campbell *et al.,* 2002; Koroleva *et al.,* 2005). We transformed the *ncb-1* line stably with this construct. Figure 8 shows different cell types from the resulting line. Large nuclear bodies are visible in all cell types, in which both the NCB/At1g13030:mRFP and the U2B″:GFP are concentrated. This shows that nuclear bodies analogous to CBs were formed in the *ncb-1* line when it expressed the NCB/At1g13030 cDNA. Furthermore these structures are likely to be functional because U2B″:GFP is recruited to them. In addition these CBs that form in the 35S:NCB:mRFP transformed plants are larger than those observed in wild-type nuclei. This indicates that levels of NCB/At1g13030 protein may regulate the sizes of CBs that form in nuclei.

DISCUSSION

We have identified a number of mutants in which CB morphology or occurrence is altered in a mutant screen of an *Arabidopsis* line engineered to have a GFP marker for CBs. This demonstrates that this type of screen using epifluorescence microscopy is effective in identifying genes that control the formation of subcellular structures. It is striking that at least three of the six mutants identified carried alterations to the same gene. The clearest phenotype among these mutants was a complete absence of CBs in the *ncb-1* mutant in all the cell types examined. We identified the gene responsible for the *ncb-1* phenotype and showed that it encodes a protein with limited homology to vertebrate coilin and is in fact the closest homologue to coilin present in the *Arabidopsis* genome. The screen also identified two mutants with other CB phenotypes, suggesting that at least two other loci may also affect CBs. In *pcb* there were significantly higher numbers of CBs. It is known that many CBs are nucleated early in G1 and that the CBs fuse during the course of interphase (Boudonck *et al.,* 1999). Thus *pcb* may be altered either in the number of CBs nucleated or in the dynamics of their fusion. The flattened CBs seen in the *ccb* are also interesting and may indicate a change in phosphorylation status of CB components (e.g., Lyon *et al.,* 1997).

A similar approach could be used in screens for factors affecting other subcellular or subnuclear structures, provided that the structures can be easily visualized by GFP fusions and can be quickly assessed by limited fluorescence microscopy of easily accessible cell types. In particular, our results show that this type of open-ended screening approach may be very useful in finding factors involved in localization or trafficking of snRNPs. In the present screen it was important to use the large and easily visible hypocotyl cells and to limit exposure of the rest of the seedling to the high-intensity microscope excitation light, which can easily cause irreversible damage to other parts of the plant. Other more subtle phenotypes in CB activity or dynamics may have been produced, but would not have been detected by our simple microscopy screen.

Coilin is known to be concentrated in CBs in a range of vertebrates, including mammals and amphibians, and is now widely regarded as diagnostic for this subnuclear organelle (Gall, 2000, 2003; Ogg and Lamond, 2002; Matera, 2003; Cioce and Lamond, 2005). However, the biochemical activity of coilin is still not fully understood. One major role appears to be directly in the formation of CBs. In support of this, a mouse coilin "knockout" line lacks normal CBs and shows only residual CB-like structures, which fail to recruit SMN protein and which therefore are not fully functional (Tucker *et al.,* 2001). The phenotype of the *Arabidopsis ncb-1* mutant indicates that coilin is absolutely required for the formation of CBs because no CBs are seen in any cell type examined in plants homozygous for the *ncb-1* mutation. Thus we can identify this *Arabidopsis* gene as a clear homologue of the vertebrate coilin gene, both on the basis of (limited) structural homology and of functional correspondence in being required for CB formation. Subsequently we refer to the protein encoded as Atcoilin.

Both *ncb-1* and *ncb-2* have point mutations at splice sites, and each gives rise to two aberrantly spliced mRNAs. In the case of *ncb-1,* the spliced mRNAs are predicted to produce substantially altered proteins either lacking the correct C-terminal sequences or containing extraneous internal residues. In the case of *ncb-2* one of the aberrantly spliced mRNAs is predicted to produce a protein lacking only two amino acid residues, but otherwise correct. This is likely to be the reason that this mutant exhibits some CBs, although smaller than the wild type. The decrease in CB size may be because the deletion of the two residues in the predicted protein impairs its function to some extent. Alternatively, it may be that this variant is fully functional, but that, representing only about half the spliced mRNA, the level of the protein is reduced. In the *ncb-3* mutant a single amino acid change from aspartate to lysine was identified. Again, this mutation, which introduces a charge alteration, may impair Atcoilin activity and thus cause the observed reduction in CB size.

The idea that levels of coilin protein determine size of CBs is supported by expressing Atcoilin cDNA in transgenic *Arabidopsis* plants under the control of the strong constitutive 35S promoter, which would be expected to lead to overexpression of Atcoilin. In these plants the CBs are greatly increased in size in all cells examined. Thus we have obtained the full spectrum of CB size, from complete absence through reduced size to great enlargement, simply by changing Atcoilin or its expression level. In this respect, Atcoilin seems to differ from mammalian coilins. When human coilin was expressed at high levels in HeLa cells, the CBs were disrupted (Shpargel *et al.,* 2003). A similar result was obtained when mouse coilin was overexpressed in mouse cells. However, overexpression of mouse coilin in HeLa cells produced an increased number of CB-like foci, although not of increased size.

We have clearly demonstrated that functional full-length Atcoilin is necessary for formation of CBs in *Arabidopsis*. Equally, we have found no obvious growth phenotype in the mutant lacking observable CBs, so that CBs cannot be essential for viability. Similarly, not all mammalian cell types or cell lines have observable CBs, and the progeny of the mouse coilin deletion mutant appeared to develop normally with only residual CBs lacking full functionality (although the litter size was reduced; Tucker *et al.*, 2001). However, the conservation of this structure across such as wide phylogenetic range from vertebrates to plants suggests that it must confer significant selective advantages. We can only speculate what these advantages may be as yet, but the most likely suggestion is that of concentrating particular nuclear components, either RNA species or proteins or both, together in a small subnuclear volume so as to increase the probability and thus efficiency of their interactions (see, e.g., Shaw and Brown, 2004; Tucker and Matera, 2005). If this were the case, we would predict that in a genetic background lacking CBs, such as *ncb-1*, the levels of such interacting factors would be altered. Either the levels of complexes or modifications produced by such interactions (e.g., RNA methylation or pseudouridylation) may be reduced, or alternatively the expression levels of limiting interacting factors may be increased to compensate for the reduction of probability of interaction. This is likely to be a fruitful area for investigation of both *ncb-1* and the mouse coilin knockout line. As regards coilin itself neither our studies nor those in other species can formally eliminate the possibility that at least the N terminal part of coilin is essential for viability, because the currently available mutant lines in both *Arabidopsis* and in mouse (Tucker *et al.*, 2001) may not be true null mutants and may express N terminal coilin fragments.

How far the functional homology between animal and plant coilins extends is an interesting question that requires more research in both kingdoms. The sequence similarity between the animal and plant proteins is restricted to the N and C terminal regions; the region in between, the major part of the protein, shows no significant similarity (Figure 5; Tucker and Matera, 2005). It is clear that the formation of CBs is likely to depend on self-association of coilin and that the N terminal region, in which significant conservation between plants and animals is seen, is important for this (Hebert and Matera, 2000). The known animal coilins have an internal region of repeated arginine and glycine residues, termed the RG domain. Matera and colleagues have shown that the arginine residues are post-translationally modified to symmetrical dimethyl arginines (Hebert *et al.*, 2001, 2002) and that this domain is involved in interaction with the core spliceosomal protein SMN. Furthermore the interaction between the methylated RG domain and SMN is in turn involved in the interaction between CBs and gem nuclear bodies, which contain SMN. Interestingly, Atcoilin does not contain an RG domain, and it is currently not known whether any of the arginine residues in Atcoilin are dimethylated. Similarly, no homologue of SMN has currently been identified in the *Arabidopsis* genome. Thus both SMN and its cognate binding site may have diverged too far to be recognizable in *Arabidopsis*.

Nevertheless, the fact, that CBs are found in both plants and animals, contain, as far as is known, similar components, and are dependent on recognizably similar proteins for their formation strongly suggest that they have diverged from a common precursor, rather than being the product of convergent evolution. Such a common precursor structure is likely to have been present in the common ancestors of plants and animals and must represent a very ancient structure in the early eukaryotes. This in turn suggests that, although individual groups of organisms may have lost CBs, they are likely to be present throughout higher eukaryotes in some form. Thus, although the biochemical processes being carried in CBs are still not fully understood, it is likely that CBs are fundamentally important in eukaryotic biology.

ACKNOWLEDGMENTS

We thank Sue Bunnewell for expert transmission electron microscopy. This work was supported by the Biotechnology and Biological Sciences Research Council of the United Kingdom and by the Marie Curie Fellowship Programme of the European Union.

REFERENCES

Acevedo, R., Samaniego, R., and Moreno Diaz de la Espina, S. (2002). Coiled bodies in nuclei from plant cells evolving from dormancy to proliferation. Chromosoma *110*, 559–569.

Andrade, L. E., Chan, E. K., Raska, I., Peebles, C. L., Roos, G., and Tan, E. M. (1991). Human autoantibody to a novel protein of the nuclear coiled body: immunological characterization and cDNA cloning of p80-coilin. J. Exp. Med. *173*, 1407–1419.

Bell, C. J., and Ecker, J. R. (1994). Assignment of 30 microsatellite loci to the linkage map of *Arabidopsis*. Genomics *19*, 137–144.

Beven, A. F., Simpson, G. G., Brown, J. W., and Shaw, P. J. (1995). The organization of spliceosomal components in the nuclei of higher plants. J. Cell Sci. *108*, 509–518.

Boudonck, K., Dolan, L., and Shaw, P. J. (1999). The movement of coiled bodies visualized in living plant cells by the green fluorescent protein. Mol. Biol. Cell *10*, 2297–2307.

Campbell, R. E., Tour, O., Palmer, A. E., Steinbach, P. A., Baird, G. S., Zacharias, D. A., and Tsien, R. Y. (2002). A monomeric red fluorescent protein. Proc. Natl. Acad. Sci. USA *99*, 7877–7882.

Cioce, M., and Lamond, A. I. (2005). Cajal bodies: a long history of discovery. Annu. Rev. Cell Dev. Biol. *21*, 105–131.

Darzacq, X., Jady, B. E., Verheggen, C., Kiss, A. M., Bertrand, E., and Kiss, T. (2002). Cajal body-specific small nuclear RNAs: a novel class of 2′-O-methylation and pseudouridylation guide RNAs. EMBO J. *21*, 2746–2756.

Dundr, M., Hebert, M. D., Karpova, T. S., Stanek, D., Xu, H., Shpargel, K. B., Meier, U. T., Neugebauer, K. M., Matera, A. G., and Misteli, T. (2004). In vivo kinetics of Cajal body components. J. Cell Biol. *164*, 831–842.

Gall, J. G. (2000). Cajal bodies: the first 100 years. Annu. Rev. Cell Dev. Biol. *16*, 273–300.

Gall, J. G. (2003). The centennial of the Cajal body. Nat. Rev. Mol. Cell. Biol. *4*, 975–980.

Gall, J. G., Tsvetkov, A., Wu, Z., and Murphy, C. (1995). Is the sphere organelle/coiled body a universal nuclear component? Dev. Genet. *16*, 25–35.

Hebert, M. D., and Matera, A. G. (2000). Self-association of coilin reveals a common theme in nuclear body localization. Mol. Biol. Cell *11*, 4159–4171.

Hebert, M. D., Shpargel, K. B., Ospina, J. K., Tucker, K. E., and Matera, A. G. (2002). Coilin methylation regulates nuclear body formation. Dev. Cell *3*, 329–337.

Hebert, M. D., Szymczyk, P. W., Shpargel, K. B., and Matera, A. G. (2001). Coilin forms the bridge between Cajal bodies and SMN, the spinal muscular atrophy protein. Genes Dev. *15*, 2720–2729.

Jady, B. E., and Kiss, T. (2001). A small nucleolar guide RNA functions both in 2′-O-ribose methylation and pseudouridylation of the U5 spliceosomal RNA. EMBO J. *20*, 541–551.

Koroleva, O. A., Tomlinson, M. L., Leader, D., Shaw, P., and Doonan, J. H. (2005). High-throughput protein localization in *Arabidopsis* using Agrobacterium-mediated transient expression of GFP-ORF fusions. Plant J. *41*, 162–174.

Lafontaine, J. G. (1965). A light and electron microscope study of small spherical nuclear bodies in meristematic cells of *Allium cepa*. J. Cell Biol. *26*, 1–17.

Lyon, C. E., Bohmann, K., Sleeman, J., and Lamond, A. I. (1997). Inhibition of protein dephosphorylation results in the accumulation of splicing snRNPs and coiled bodies within the nucleolus. Exp. Cell Res. *230*, 84–93.

Matera, A. G. (2003). Cajal bodies. Curr. Biol. *13*, R503.

Monneron, A., and Bernhard, W. (1969). Fine structural organization of the interphase nucleus in some mammalian cells. J. Ultrastruct. Res. *27*, 266–288.

Nesic, D., Tanackovic, G., and Kramer, A. (2004). A role for Cajal bodies in the final steps of U2 snRNP biogenesis. J. Cell Sci. *117*, 4423–4433.

Ogg, S. C., and Lamond, A. I. (2002). Cajal bodies and coilin—moving towards function. J. Cell Biol. *159*, 17–21.

Platani, M., Goldberg, I., Swedlow, J. R., and Lamond, A. I. (2000). In vivo analysis of Cajal body movement, separation, and joining in live human cells. J. Cell Biol. *151*, 1561–1574.

Ramon y Cajal, S. (1903). Un sencillo metodo de coloracion seletiva del reticulo protoplasmatico y sus efectos en los diversos organos nerviosos de vertebrados e invertebrados. Trab. Lab. Invest. Biol. (Madrid) *2*, 129–221.

Raska, I., Andrade, L.E.C., Ochs, R. L., Chan, E.K.L., Chang, C. M., Roos, G., and Tan, E. M. (1991). Immunological and ultrastructural studies of the nuclear coiled body with autoimmune antibodies. Exp. Cell Res. *195*, 27–37.

Schaffert, N., Hossbach, M., Heintzmann, R., Achsel, T., and Luhrmann, R. (2004). RNAi knockdown of hPrp31 leads to an accumulation of U4/U6 di-snRNOs in Cajal bodies. EMBO J. *23*, 3000–3009.

Shaw, P. J., and Brown, J. W. (2004). Plant nuclear bodies. Curr. Opin. Plant Biol. *7*, 614–620.

Shpargel, K. B., Ospina, J. K., Tucker, K. E., Matera, A. G., and Hebert, M. D. (2003). Control of Cajal body number is mediated by the coilin C-terminus. J. Cell Sci. *116*, 303–312.

Sleeman, J. E., Trinkle-Mulcahy, L., Prescott, A. R., Ogg, S. C., and Lamond, A. I. (2003). Cajal body proteins SMN and Coilin show differential dynamic behaviour in vivo. J. Cell Sci. *116*, 2039–2050.

Stanek, D., and Neugebauer, K. M. (2004). Detection of snRNP assembly intermediates in Cajal bodies by fluorescence resonance energy transfer. J. Cell Biol. *166*, 1015–1025.

Tucker, K. E., Berciano, M. T., Jacobs, E. Y., LePage, D. F., Shpargel, K. B., Rossire, J. J., Chan, E. K., Lafarga, M., Conlon, R. A., and Matera, A. G. (2001). Residual Cajal bodies in coilin knockout mice fail to recruit Sm snRNPs and SMN, the spinal muscular atrophy gene product. J. Cell Biol. *154*, 293–307.

Tucker, K. E., and Matera, A. G. (2005). The Cajal body—a nuclear gathering place. In: Visions of the Nucleus, ed. P. Hemmerich, S. Diekmann, Stevenson Ranch, CA: American Scientific Publishers, 159–171.

Tuma, R. S., Stolk, J. A., and Roth, M. B. (1993). Identification and characterization of a sphere organelle protein. J. Cell Biol. *122*, 767–773.

Verheggen, C., Mouaikel, J., Thiry, M., Blanchard, J. M., Tollervey, D., Bordonne, R., Lafontaine, D. L., and Bertrand, E. (2001). Box C/D small nucleolar RNA trafficking involves small nucleolar RNP proteins, nucleolar factors and a novel nuclear domain. EMBO J. *20*, 5480–5490.

Zhu, Y., Tomlinson, R. L., Lukowiak, A. A., Terns, R. M., and Terns, M. P. (2004). Telomerase RNA accumulates in Cajal bodies in human cancer cells. Mol. Biol. Cell *15*, 81–90.